A Quantum Molecular Dynamics Simulation Study of the Initial Hydrolysis Step in Sol−Gel Process

Mohamed Elanany,[†] Parasuraman Selvam,[‡,||] Toshiyuki Yokosuka,[†] Seiichi Takami,[†] Momoji Kubo,[†] Akira Imamura,[§] and Akira Miyamoto*[,†,‡]

Department of Materials Chemistry, Graduate School of Engineering, Tohoku University, Aoba-yama 07, Sendai 980-8579, Japan, Department of Mathematics, Faculty of Engineering, Hiroshima Kokusai Gakuin University, 6-20-1 Nakano, Aki-ku, Hiroshima 739-0312, Japan, New Industry Creation Hatchery Center (NICHe), Tohoku University, Aoba-yama 04, Sendai 980-8579, Japan

Received: August 22, 2002; In Final Form: December 10, 2002

The dynamic behavior of the hydrolysis reaction of $Si(OCH_3)_4$ under neutral, basic, and acidic conditions was investigated, for the first time, at the atomic level with short time intervals using a novel tight-binding quantum chemical molecular dynamics program "Colors". The initial parameters required for the computation were determined completely on the basis of the first principles density functional calculations using Amsterdam density functional program. The simulation results of this study clearly indicate that a flank-side attack mechanism is favored, in all the three cases, for the hydrolysis process, and pentacoordinate silicon intermediates are easy pathways for the displacement of $-OCH_3$ by $-OH$ on silicon. Moreover, the presence of the acid or the base as catalyst promotes the hydrolysis by rapid formation of Si−OH bond in comparison to the hydrolysis under neutral condition. Furthermore, in the case of the latter condition, it was observed that the proton oscillates between $-OH$ and $-OCH_3$ before it migrates to the latter group.

1. Introduction

Computational quantum chemistry provides a detailed description of the bonding, charge distribution, structural preferences, and geometry of molecular materials. Recently, the computational quantum chemistry has extensively been applied to describe complicated reactions such as sol−gel process and hydrothermal synthesis of porous materials. The study of the hydrolyses of metal alkoxides, $M(OR)_n$, is very important as they are fundamental reactions in the sol−gel processes, given that sol−gel processing of alkoxysilanes and organoalkoxysilanes is a promising technology for the production of certain industrially important advanced materials and coatings, e.g., glasses, ceramics, microporous (zeolites), and mesoporous molecular sieves, etc. Silicon alkoxides, $Si(OR)_4$, such as tetramethoxysilane, $Si(OCH_3)_4$, and tetraethoxysilane, $Si(OC_2H_5)_4$, are commonly employed as molecular precursors for sol−gel processing of silica[1] owing to their high solubility in common organic solvents, ease in purification, low temperature preparation, excellent homogeneity of the products obtained, as well as their usefulness in the formation of pure oxides. In general, metal alkoxides react readily with water and hydrolyze rapidly.

$$M(OR)_4 + H_2O \rightarrow M(OR)_3(OH) + ROH \qquad (1)$$

However, depending on the amount of water and the catalyst present, the hydrolysis may go to completion or stop while it is only partially hydrolyzed. At this juncture, it is, also noteworthy here that silicon alkoxides are less reactive than the corresponding transition metal alkoxides and hence acids or bases are often used as catalysts for promoting the hydrolysis and the subsequent condensation (polymerization) reactions. On the other hand, it has been demonstrated that the reaction of isotopically labeled water ($H_2{}^{18}O$) with $Si(OC_2H_5)_4$ produces only unlabeled alchohols in both acidic and basic conditions,[2] thus supporting the hypothesis of a nucleophilic attack of the oxygen of water.

$$Si(OR)_4 + H_2{}^{18}O \rightarrow Si(OR)_3({}^{18}OH) + ROH \qquad (2)$$

In the past, several mechanisms have been put forward for the hydrolysis of the $Si(OR)_4$.[2−17] For both acid- (eq 3) and base-catalyzed (eq 4) reactions, a S_N2-type backside displacement (with inversion) path was proposed.[2] Other groups[9,10,17] have suggested a flank-side attack mechanism (eq 5) or retention (without inversion) mechanism for the acid-promoted hydrolysis process. However, S_N2-type mechanism involving a stable pentacoordinate intermediate with two trasition states has also been proposed under basic conditions.[4,9]

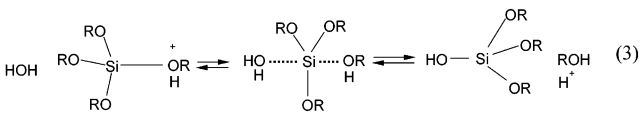

(3)

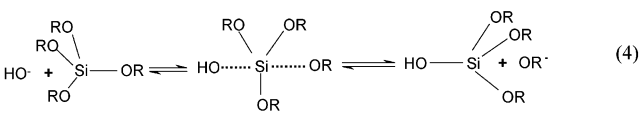

(4)

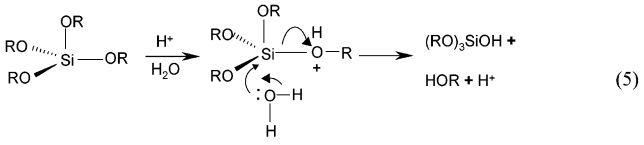

(5)

* Corresponding author. E-mail: miyamoto@aki.che.tohoku.ac.jp.
[†] Department of Materials Chemistry, Tohoku University.
[||] On sabbatical leave from Department of Chemistry, Indian Institute of Technology-Bombay, Powai, Mumbai 400 076, India.
[‡] New Industry Creation Hatchery Center, Tohoku University.
[§] Department of Mathematics, Hiroshima Kokusai Gakuin University.

10.1021/jp026816z CCC: $25.00
Published on Web 01/24/2003

Timms[11] has proposed yet another mechanism under acidic condition involving a siliconium ion intermdediate (eq 6). That is, in the presence of the acid, the alkoxide group is rapidly protonated followed by a slower step in which the siliconium ion $Si(OR)_3^+$ is formed by the removal of alcohol. The $Si(OR)_3^+$ then reacts with water to form the silanol. Although the

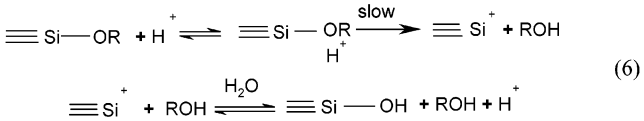

(6)

hydrolysis mechanism under neutral condition is still unclear, a recent computational study by Okumoto et al.[4] support a front-side nucleophilic attack, i.e., the alkoxide hydrolyze without inversion, which is in contrast to the backside attack mechanism considered for the acid- and base-catalyzed hydrolysis reaction.

Numerous experimental and theoretical investigations have focused on the consequences as well as the validity of the various available mechanisms for the hydrolysis process.[2−7,10−16] The possible effect of inversion of silicon tetrahedron with respect to retarding the hydrolysis of silicate species is discussed. It was also stated that the inverstion or retention may occur in displacement reactions depending on the nature of the catalyst and the solvent polarity, with poor leaving groups, such as H or OR, whose conjugate acids have $pK_a > 6$. On the other hand, Corriu and Henner[12] have examined the feasibility of siliconium ion model for the hydrolysis by various physicochemical methods as well as by preparation of stable salts or by identification of reaction intermediates but failed to prove its existence. However, on the bases of ^{29}Si nuclear magnetic resonance and vibrational spectroscopic studies,[13−15] it was deduced that the hydrolysis of $Si(OCH_3)_4$ proceeds through an associative mechanism involving a pentacoordinate silicon intermediate (eqs 3−5) rather than a dissociative mechanism in which a tricoordinate siliconium ion is formed as an intermediate (eq 6). The former is well-supported by Swain et al.[16] They compared the hydrolysis behavior of both triphenylsilylflouride and triphenylmethylflouride, and suggested the feasibility of the formation of a pentacoordinate intermediate for silicon in contrast to carbon.

In view of the existing discrepancies of the different pathways for the hydrolysis of silicon alkoxides as well as the importance of the sol−gel reactions in the processing of the silicon-based advanced materials, in this investigation, an attempt was made to provide a better description and get further insight into the hydrolysis process using a molecular dynamics method. Although sevaral theoretical studies employing various levels of approximations have been performed, the results of these studies, however, do not project the dynamics effect[3−5] as well as the electronic interactions (bond formation and/or bond cleavage).[6−8] This prompted us to carry out the study of the dynamic behavior of the hydrolysis of $Si(OCH_3)_4$ at the atomic level with very short time intervals. Thus, the present work focuses on the molecular dynamics simulation of the initial hydrolysis step under different conditions, viz., acidic, basic, and neutral, using a novel accelerated tight-binding quantum chemical molecular dynamics program "Colors".[18,19]

2. Computaional Details

2.1. Theory. In the tight-binding quantum chemical molecular dynamics program "Colors", the total energy between any pair of atoms, designated as *i* and *j*, is given by the following expression:

$$E = \sum_{i=1}^{n} m_i v_i^2/2 + \sum_{k=1}^{occ} \epsilon_k + \sum\sum_{i>j} Z_i Z_j e^2/R_{ij} + \sum\sum_{i>j} E_{rep}(R_{ij}) \quad (7)$$

where the first, second, third, and fourth terms represent the kinetic energy, the summation of the eignvalues of all occupied orbital (orbital energy of valence electrons), the Coulombic interaction energy, and the exchange−repulsion interaction energy, respectively. Here, *m* and *v* are mass and velocity of atoms, Z_i and Z_j are the charges of atoms, *e* is the elementary electric charge, and R_{ij} is the internuclear distance. The exchange−repulsion term, $E_{rep}(R_{ij})$ is given by

$$E_{rep}(R_{ij}) = b_{ij} \exp[(a_{ij} - R_{ij})/b_{ij}] \quad (8)$$

where the parameters *a* and *b* represent the sum of the size and stiffness of the atoms, *i* and *j*, respectively. On the other hand, the following equation describes the force

$$F_i = \sum_{j\neq i}^{n}\sum_{k=1}^{occ} C_k^T(\partial H/\partial R_{ij})C_k + \sum_{j\neq i}^{n}\sum_{k=1}^{occ} \epsilon_k C_k^T(\partial S/\partial R_{ij})C_k - \sum_{j\neq i} Z_i Z_j e^2/R_{ij}^2 + \sum_{j\neq i} \partial E_{rep}(R_{ij})/\partial R_{ij} \quad (9)$$

where *H* is the Hamiltonian matrix, *C* is the eignvector matrix, and C^T is the transformation matrix of the eignvector matrix. Higher accuracy was achieved by our new parametrization procedure based on the first principles density functional theory (DFT) calculations. We employed parameters such as the Slater exponent of each atomic orbital in order to accelerate the calculation speed. Further details regarding the first principles parametrization can be seen elsewhere.[18,19] On the basis of the improvements in Wolfsberg−Helmholz formula by Anderson[20] and Calzaferri et al.,[21] we employed the following corrected distance-dependent expression, *K* for off-diagonal terms of the Hamiltonian H_{rs}:

$$H_{rs} = \frac{1}{2} K_{rs}(H_{rr} + H_{ss})S_{rs} \quad (10)$$

$$K_{rs} = 1 + (\kappa_{rs} + \Delta^2 - \Delta^4\kappa_{rs}) \exp[-\delta_{rs}(R_{ij} - d_0)] \quad (11)$$

$$\Delta = (H_{rr} - H_{ss})/(H_{rr} + H_{ss}) \quad (12)$$

where H_{rr} is the diagonal term of Hamiltonian matrix, which is equal to the first ionization energy of each atomic orbital, S_{rs} is the overlap matrix, and d_0 is the sum of the orbital radii. To improve the accuracy further, the parameters κ_{rs} and δ_{rs}, used in our tight-binding Hamiltonian, were determined to satisfy the bond lengths, binding energies, and frequencies of diatomic molecules such as SiO, CO, OH, NH, CH, etc. Furthermore, the calculations performed on different models using the molecular dynamics program "Colors" confirmed that it is much faster than (over 5000 times) the regular first principles calculations.[19]

2.2. Molecular Models and Simulation Conditions. The initial molecular structures used for the simulations, viz., $Si(OMe)_4$ and one H_2O or $H_3O^+Cl^-$ or $NH_4^+OH^-$, were determined by DFT method employing the Amsterdam density functional (ADF) program package.[22] These initial structures were geometrically optimized with the Vosko−Wilk−Nusair[23] local density approximation (LDA) whereas the energies were evaluated at the generalized gradient approximation (GGA) level with Perdew−Wang (PW91XC)[24] exchange and correlation functionals. In this investigation, molecular dynamics simula-

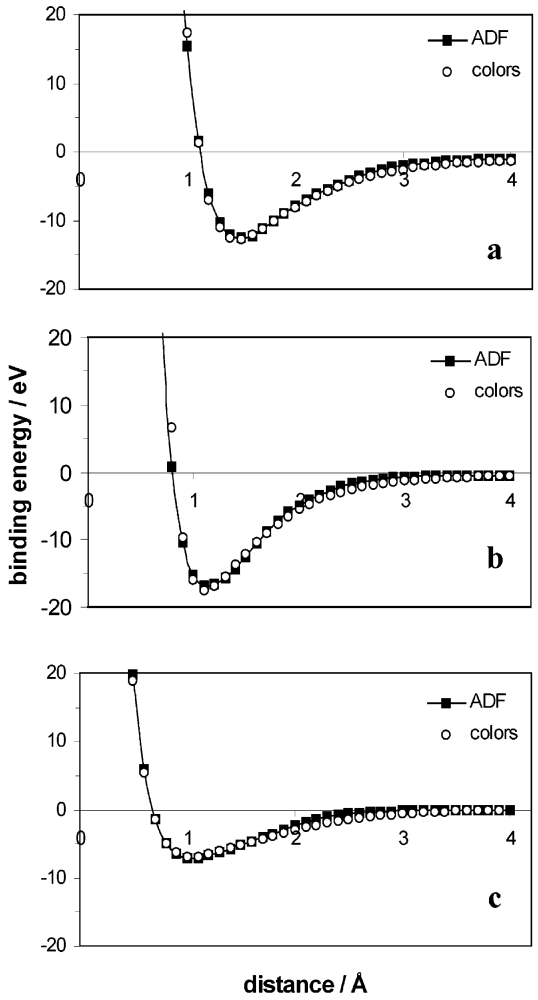

Figure 1. Diatomic potential energy curves of: (a) Si−O, (b) C−O, and (c) N−H.

tions were carried out in a vacuum at ambient pressure and temperature conditions. Cubic unit cells of size 20.0 Å × 20.0 Å × 20.0 Å were used for all models. Each unit cell contains one $Si(OMe)_4$, and one H_2O, $H_3O^+Cl^-$, and $NH_4^+OH^-$ in the case of neutral, acidic, and basic conditions, respectively. In this simulation, 2000 steps, with a time interval of 0.1 fs, were performed under the neutral and acidic conditions, while 1880 steps were used under basic condition. The various structures during the molecular dynamics simulations were visualized using RYUGA software.[25]

Parametrization for the molecular dynamics program "Colors" was carried out on the basis of DFT calculations by ADF program. Although ADF uses triple-ζ functions to describe the atomic orbital, "Colors" can demonstrate accurately the same atomic orbital with single or double-ζ Slater-type orbital employing a charge-dependent Slater exponent. Figure 1 shows the typical potential energy curves of different diatomic molecules such as SiO, CO and NH. As can be seen from this figure that the energy curves obtained both by ADF and "Colors" codes are nearly identical. It is clear from these potential energy curves that there exist strong interactions, well beyond 2 Å, for SiO (−1.24 eV at 4 Å, −2.04 eV at 3 Å, Figure 1a) and CO (−0.56 eV at 4 Å, −1.30 eV at 3 Å, Figure 1b) molecules. On the other hand, a weak interaction can be noticed for while for NH (−0.07 eV at 4 Å, Figure 1c). It is, however, noteworthy here that stronger interactions can also be noticed for NH at shorter distances (−0.59 eV at 3.0 Å, −1.40 eV at 2.5 Å, Figure 1c). Furthermore, the potential energy curves

TABLE 1: Binding Energies and Charges Calculated for Different Molecules by ADF and "Colors"

molecule	binding energy (eV)	charge distribution Si	H	O	C	program
$Si(OH)_4$	−49.72	0.56	0.15	−0.29		ADF[a]
	−47.98	0.41	0.16	−0.26		"Colors"
$Si_2O_7H_6$	−76.45	0.61	0.16	−0.31		ADF[a]
	−77.47	0.54	0.15	−0.28		"Colors"
$Si(OCH_3)_4$	−114.95	0.53	0.05	−0.20	−0.06	ADF[a]
	−114.96	0.65	0.05	−0.30	−0.01	"Colors"

[a] Hirshfeld charge.

obtained by "Colors" for other diatomic molecules (not reproduced here) such as OH, CH, HH, etc. also agree well with that obtained by ADF. It is worth mentioning here that in all these cases strong interactions prevail <2.5 Å (e.g., HH: − 1.85 eV at 2 Å, − 0.62 eV at 2.5 Å, − 0.15 eV at 3.0 Å). At this juncture, it is important to point out here that in our simulation models the actual interactions between the various atoms are taking place well below 2 Å and hence the possible bias of the DFT in describing the dispersion forces is not encountered. The parameters, viz., κ and δ, obtained for each pair of the atomic orbital of various diatomic molecules were used to calculate the energies, bond lengths, and bond population of larger molecules, such as $Si(OH)_4$ and $Si_2O_7H_6$ in addition to $Si(OCH_3)_4$, and the results are summarized in Table 1. As can be seen from this table, the values obtained by "Colors" are in good agreement with that obtained using ADF.

3. Results and Discussion

3.1. Dynamics of Hydrolysis under Neutral Condition. Figure 2 shows snapshots of the simulation of the hydrolysis reaction of $Si(OCH_3)_4$. Here, the oxygen atoms of $Si(OCH_3)_4$ are designated as O_{19}, O_{18}, O_{15}, and O_m. Likewise, the oxygen of H_2O is defined as O_w. Initially, the water molecule was placed at a distance 1.64 Å from silicon of $Si(OCH_3)_4$. The average bond lengths for Si−O, C−O and C−H during the simulation are 1.72, 1.37, and 1.20 Å, respectively. It is also clear from this figure that a flank-side attack of oxygen in water on silicon of $Si(OCH_3)_4$ (without inversion of the silicon tetrahedron) is favorable. Further, this attack makes the leaving alkoxide group diffuses away as methanol after protonation. The calculated activation energy for the hydrolysis is 22.7 kcal/mol which is comparable with the reported value (21.6 kcal/mol) of Okumoto et al.[26] Figure 3 depicts the bond population analysis of the interaction of $Si(OCH_3)_4$ and water during the simulation. It can be seen from this figure that the fortification of the $Si-O_w$ bond at the end of the simulation (or after ∼1300 steps) ensuring the completeness of the hydrolysis. It can also be noted from this figure that the $Si-O_w$ bond population is relatively high at the beginning of the simulation since it was started from the activated structure (see Figure 2b). It is interesting to note that in the midway of the simulation, the Si−O bonds' population, i.e., $Si-O_w$, $Si-O_m$, $Si-O_{15}$, $Si-O_{18}$, and $Si-O_{19}$, reveals that the formation of silicon pentacoordinate intermediate rather than siliconium ion intermediate reported previously.[11] These results indicate that the pentacoordinate intermediate is the easy pathway for the displacement of OCH_3 by OH on $Si(OCH_3)_4$. Figure 4 illustrates the proton oscillations (∼60 fs) between O_w and O_m during the simulation. However, after this oscillation period, the proton migrates to the O_m to form methanol. Laasonen and Klein[27] have also made a similar observation earlier for hydrochloric acid−water system and related these fluctuations to the change in the coordination number of chloride ions.

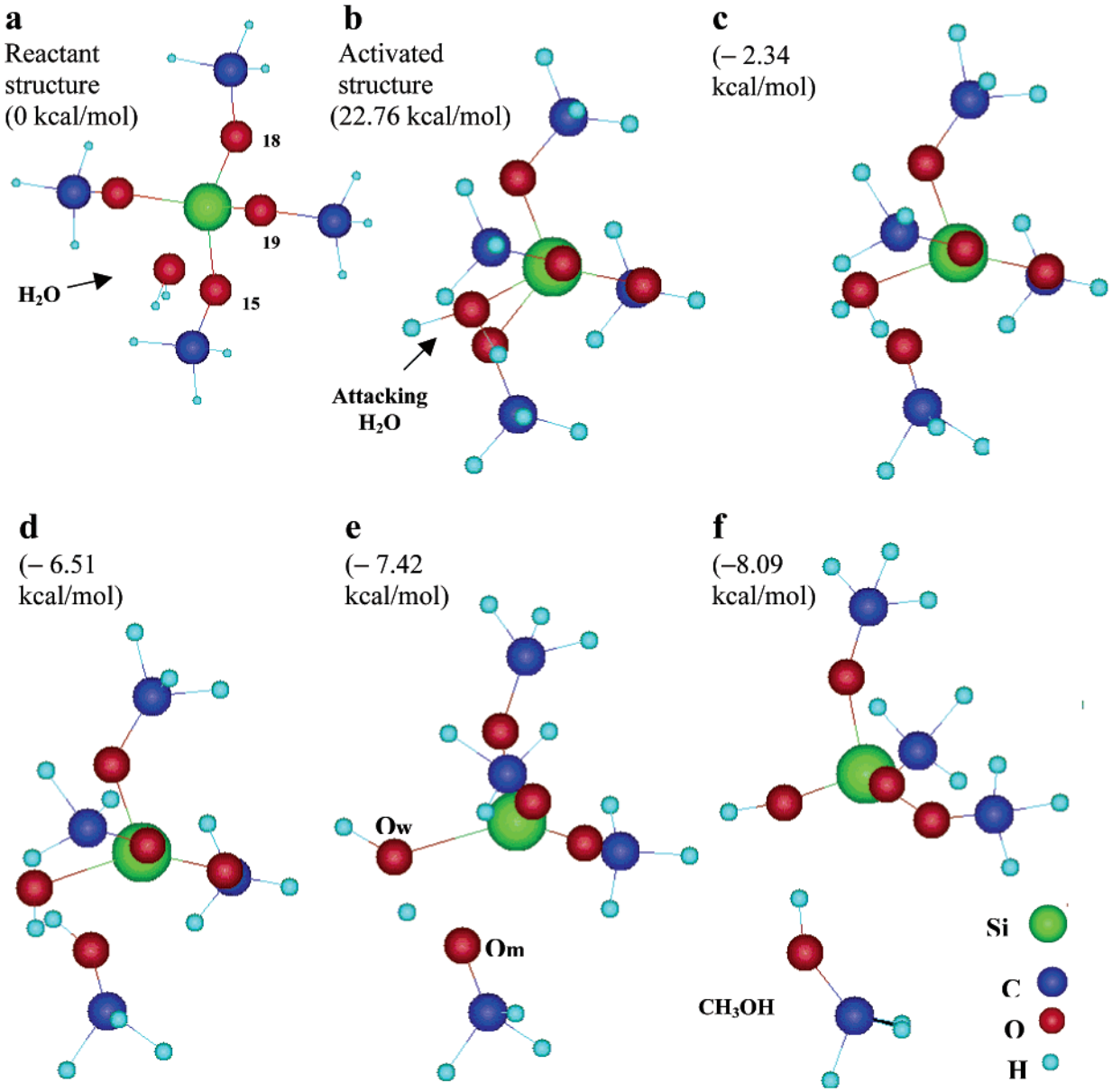

Figure 2. Snapshots taken during the hydrolysis reaction of $Si(OCH_3)_4$ under neutral condition at various steps: (a) 50, (b) 280, (c) 400, (d) 910, and (e) 1680.

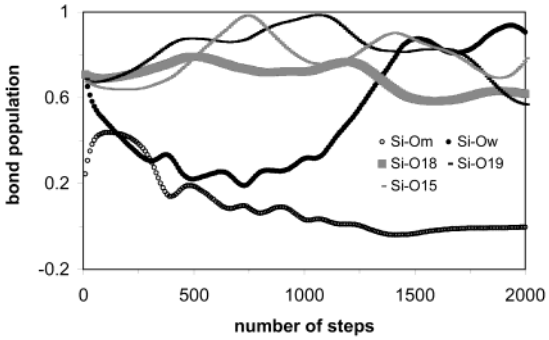

Figure 3. Bond population of silicon and its surrounding oxygen during the hydrolysis of $Si(OCH_3)_4$ under neutral condition.

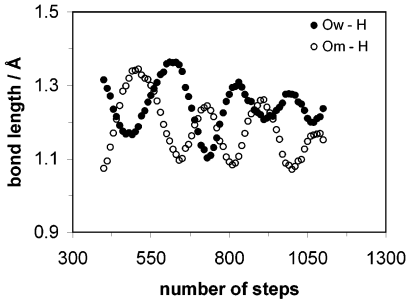

Figure 4. Bond lengths of O_w−H and O_m−H during the hydrolysis of $Si(OCH_3)_4$ under neutral condition.

3.2. Dynamics of Acid-Promoted Hydrolysis. Figure 5 depicts snapshots of the dynamics of the hydrolysis of $Si(OCH_3)_4$ under acidic condition. In this case, the oxygen atoms of $Si(OCH_3)_4$ are defined as O_{18}, O_{19}, O_{20}, and O_m. Initially, the oxygen of $H_3O^+Cl^-$ (O_w) was placed at a distance of 1.72 Å from silicon. It can be seen from this figure that, at the beginning of the simulation, the methoxy group is protonated followed by the attack of the nucleophile. Subsequently, the methoxy group diffuses away rapidly from the substrate molecule as methanol. Furthermore, at the end of the simulation, the structural rearrangement of the hydrolyzed species, $SiOH(OCH_3)_3$, can be noticed. Figure 6 shows the bond population of silicon and its surrounding oxygen atoms during the simulation. The

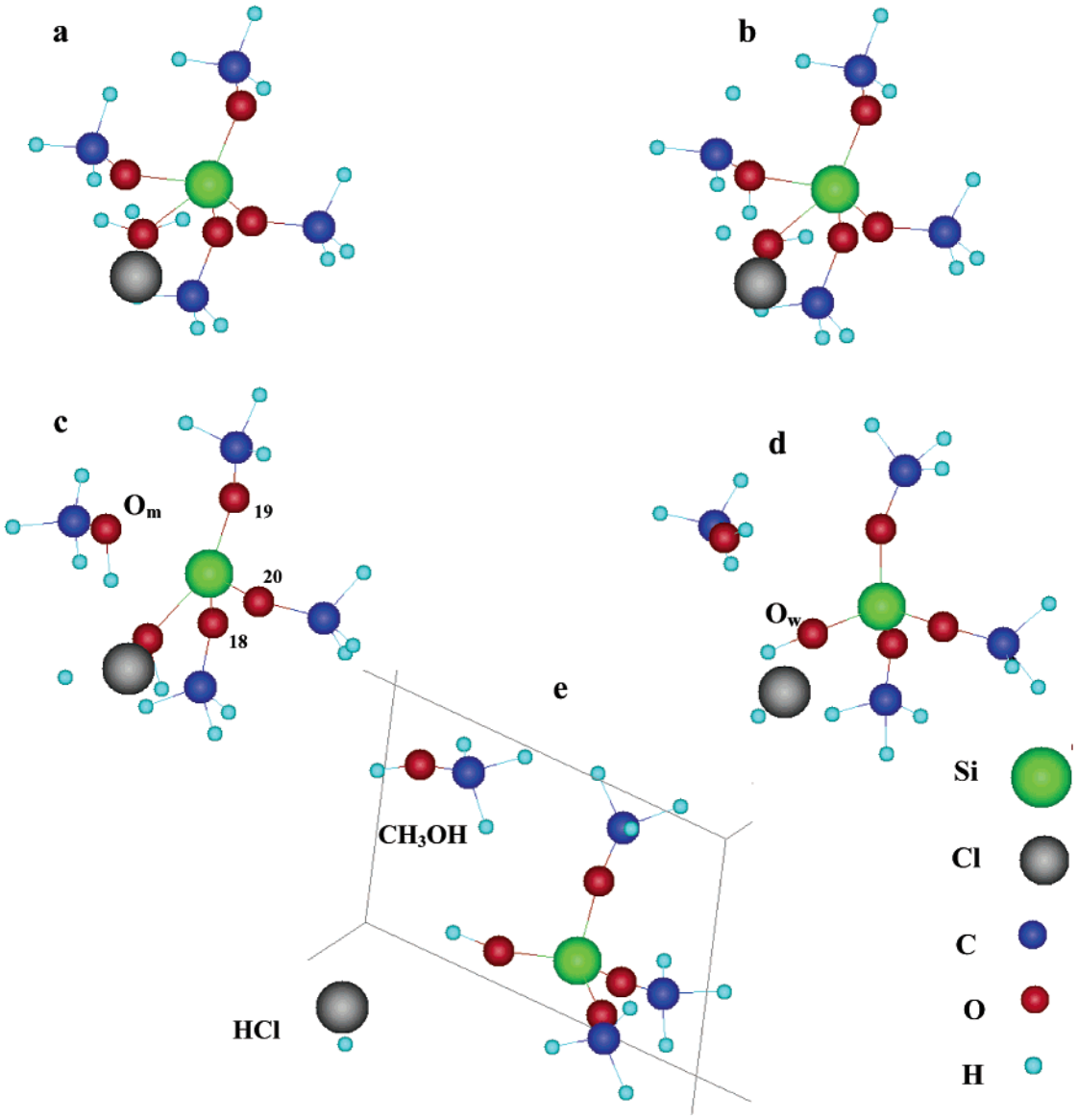

Figure 5. Snapshots taken during the hydrolysis reaction of $Si(OCH_3)_4$ under acidic condition at different steps: (a) 40, (b) 90, (c) 560, (d) 1190, and (e) 1960.

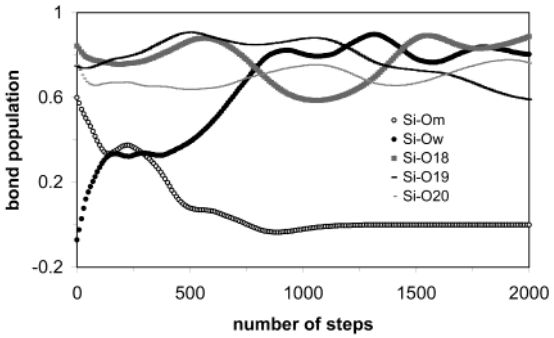

Figure 6. Bond population of silicon and its surrounding oxygen during the hydrolysis of $Si(OCH_3)_4$ under acidic condition.

contributions from different oxygen atoms to form Si−O bonds indicate the formation of silicon pentacoordinate intermediate during the hydrolysis reaction. In this context, it is noteworthy here that the contributions from O_w and O_m are weaker than that from other oxygen atoms. It is also interesting to note form this figure that there is a rapid formation of Si−O_w bond at the beginning of the hydrolysis, which was not observed under neutral condition (see Figure 3). This undoubtedly reflects the catalytic effect of the acid on the hydrolysis reaction of $Si(OCH_3)_4$.

3.3. Dynamics of Base-Promoted Hydrolysis. Figure 7 presents snapshots of the hydrolysis of $Si(OCH_3)_4$ under the basic condition at various steps where the oxygen atoms are labeled as O_{18}, O_{20}, O_{21}, and O_m. The initial distance between O_w in the attacking nucleophile ($NH_4^+OH^-$) and silicon in $Si(OCH_3)_4$ molecule was 1.71 Å. It can be seen from this figure that at the beginning of the reaction, the nucleophile attacks silicon followed by protonation of the adjacent methoxy group, which in turn leaves as methanol. Figure 8 shows the bond population of silicon with its surrounding oxygen atoms. It is interesting to note here that at the initial stage of hydrolysis, the nucleophile is quite far (1.71 Å) from the $Si(OCH_3)_4$ molecule, and the Si−O_w population has a negative value (close to zero) indicating that there is not enough interaction between the nucleophile and the substrate molecule for form Si−O_w bond. A similar trend was also noticed under the acidic condition (see Figure 6). However, when the nucleophile approaches closer to $Si(OCH_3)_4$, the bond population of Si−O_w increases rapidly, owing to the catalytic effect of the base, suggesting the hydrolysis reaction takes place instantly, which is in contrast

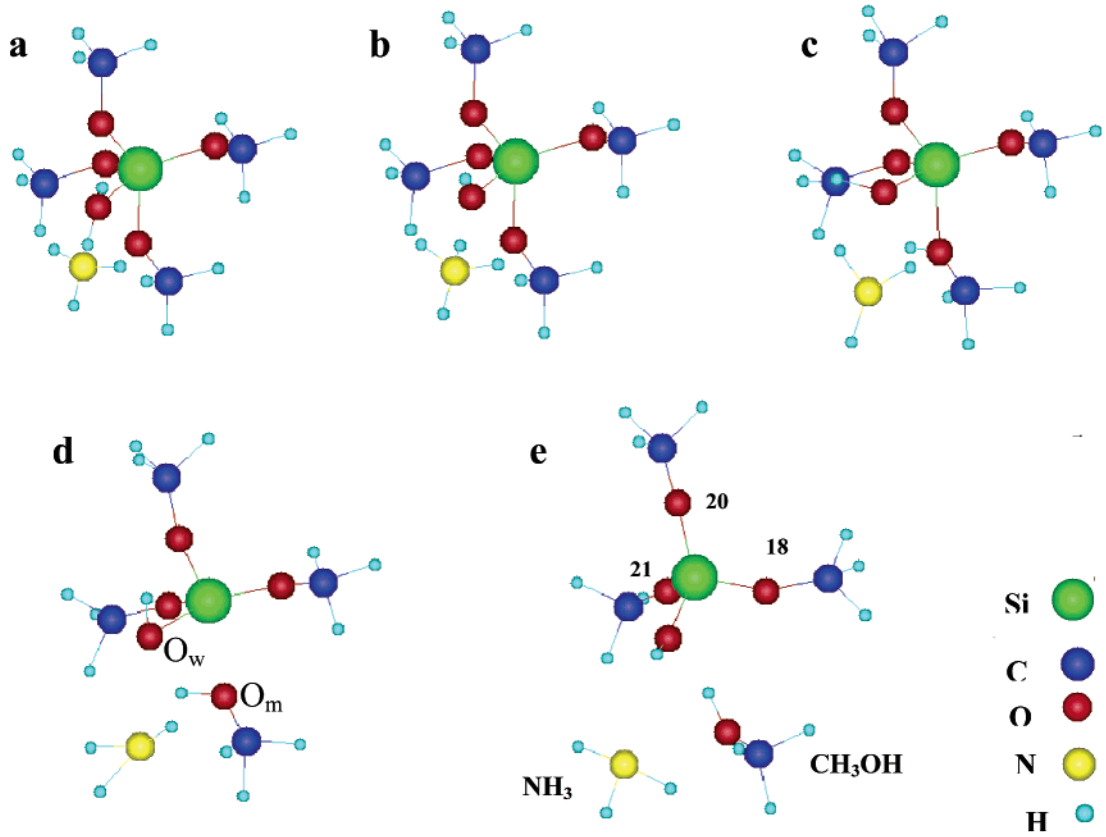

Figure 7. Snapshots taken during the hydrolysis reaction of $Si(OCH_3)_4$ under basic condition at various steps: (a) 10, (b) 50, (c) 240, (d) 570, and (e) 1690.

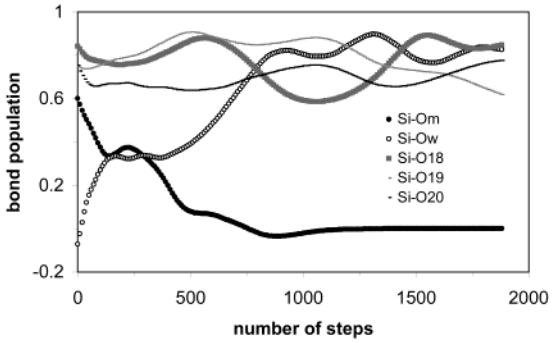

Figure 8. Bond population of silicon and its surrounding oxygen during the hydrolysis of $Si(OCH_3)_4$ under basic condition.

to the hydrolysis under neutral condition (see Figure 3). In this context, it is also noteworthy here that at the middle of the simulation, all the five oxygen atoms around the silicon have enough contributions to form a pentacoordinate intermediate.

4. Conclusions

In summary, the novel molecular dynamic simulation study enabled us to present a clear view of the interatomic interactions during the hydrolysis of $Si(OCH_3)_4$ under neutral, acidic and basic conditions. It is deduced from this investigation that, irrespective of the reaction conditions, a flank-side attack mechanism (S_N2-type without inversion) is favorable during the hydrolysis reaction of $Si(OCH_3)_4$. Moreover, the bond population analyses under different reaction conditions showed contributions from all oxygen atoms around silicon to form Si−O bonds indicating that pentacoordinate intermediates are easy pathways for the displacement of $-OCH_3$ by $-OH$ on silicon, which is in contrast to the tricoordiante siliconium ion formation mechanism. Furthermore, the presence of the acid or the base as catalyst promotes the hydrolysis by the rapid formation of Si−OH bond. In addition, in the case of hydrolysis under neutral condition, the proton oscillates for a period of ∼60 fs between oxygen of water and oxygen of leaving methoxy group where it finally migrates to the latter to form methanol. However, it is likely that under realistic conditions of hydrolysis, the polarity as well as the concentration of the solvent may have an influence on the type of the hydrolysis mechanism. Further work is in progress in order to simulate the hydrolysis process under such conditions.

References and Notes

(1) Aegerter, M. A.; Jafelicci, M.; Souza, D. F.; Zanotto, E. D. *Sol−Gel Science and Technology*; World Scientific Publishing: Singapore, 1989.
(2) Brinker, C. J.; Scherer, G. W. *Sol−Gel Science: The Physics and Chemistry of Sol−Gel Processing*; Academic Press: London, 1990.
(3) Ermoshin, V. A.; Smirnov, K. S.; Bougeard, D. *J. Mol. Struct.* **1997**, *393*, 171.
(4) Okumoto, S.; Fujita, N.; Yamabe, S. *J. Phys. Chem.* **1998**, *102*, 3991.
(5) Field, R. J.; Olson, E. W. *J. Non-Cryst. Solids* **2001**, *285*, 194.
(6) Garofalini, S. H.; Martin, G. *J. Phys. Chem.* **1994**, *98*, 1311.
(7) Martin, G.; Garofalini, S. H. *J. Non-Cryst. Solids* **1994**, *171*, 68.
(8) Pereira, J. C. G.; Catlow, C. R. A.; Price, G. D. *J. Phys. Chem.* **2002**, *106*, 130.
(9) Pohl, E. R.; Osterholtz, F. D. In *Molecular Characterization of Composite Interfaces*; Ishida, H., Kumar, G., Eds.; New York, 1985; p 157.
(10) Keefer K. D. In *Better Ceramics Through Chemistry*; Brinker, C. J., Clark, D. E., Ulrich, D. R., Eds.; New York, 1984; p 15.
(11) Timms, R. E. *J. Chem. Soc. A* **1971**, 196.
(12) Corriu, R.; Henner, M. *J. Organomet. Chem.* **1974**, *74*, 1−28.
(13) Jonas, J. In *Science of Ceramic Chemical Processing*; Hench, L. L., Ulrich, D. R. Eds.; Willy: New York, 1986; p 65.
(14) Artaki, I.; Shinha, S.; Irwin, A.; Joans, J. *J. Non-Cryst. Solids* **1985**, *72*, 391.
(15) Zerda, T.; Hoang, G. *J. Non-Cryst. Solids* **1989**, *109*, 9.

(16) Swain, C.; Esteve, R.; Joans, R. *J. Am. Chem. Soc.* **1949**, *11*, 965.
(17) Uhlmann, D.; Zelinski, B.; Wnek, G. In *Better Ceramics Through Chemistry*; Brinker, C. J., Clark, D., Ulrich, D. Eds.; North-Holland, New York, 1984; p 59.
(18) Elanany, M.; Sasata, K.; Yokosuka, T.; Takami, S.; Kubo, M.; Miyamoto, A. *Stud. Surf. Sci. Catal.* **2002**, *142*, 1867.
(19) Yokosuka, T.; Kurokawa, H.; Takami, S.; Kubo, M.; Miyamoto, A.; Imamura, A. *Jpn. J. Appl. Phys.* **2002**, *41*, 2410.
(20) Anderson, A. B. *J. Chem. Phys.* **1975**, *62*, 1187.
(21) Calzaferri, G.; Forss, L.; Kamber, I. *J. Phys. Chem.* **1989**, *93*, 5366.
(22) G. te Velde, Bickelhaupt, F. M.; Baerends, E. J.; Guerra, C. F.; Van gisbergen S. J.; Snijders, J. G.; Zieglar, T. *J. Comput. Chem.* **2001**, *22*, 931.
(23) Vosko, S. H.; Wilk, L.; Nusair, M. *Can. J. Phys.* **1980**, *58*, 1200.
(24) Perdew, J. P.; Chevary, J. A.; Vosko, S. H.; Jackson, K. A.; Pederson, M, R.; Singh D. J.; Fiolhais, C. *Phys. Rev. B* **1992**, *46*, 6671.
(25) Miura, R.; Yamano, H.; Yamauchi, R.; Katagiri, M.; Kubo, M.; Vetrivel, R.; Miyamoto, A. *Catal. Today* **1995**, *23*, 409.
(26) Okumoto, S.; Yamabe, S. *J. Non-Cryst. Solids* **2001**, *291*, 167.
(27) Laasonen, K.; Klein, M. *J. Phys. Chem. A* **1997**, *101*, 98.